Analysis of solid particles falling down and interacting in a channel with sedimentation using fictitious boundary method

Cite as: AIP Advances **8**, 065201 (2018); https://doi.org/10.1063/1.5035163
Submitted: 13 April 2018 • Accepted: 22 May 2018 • Published Online: 01 June 2018

K. Usman, K. Walayat, R. Mahmood, et al.

Analysis of solid particles falling down and interacting in a channel with sedimentation using fictitious boundary method

K. Usman,[1,a] K. Walayat,[2,a] R. Mahmood,[1,a] and N. Kousar[1,a]
[1]*Department of Mathematics, Air University, PAF Complex, Islamabad 44000, Pakistan*
[2]*Department of Mechanics and Engineering Science, College of Engineering, Peking University, Beijing 100187, China*

(Received 13 April 2018; accepted 22 May 2018; published online 1 June 2018)

We have examined the behavior of solid particles in particulate flows. The interaction of particles with each other and with the fluid is analyzed. Solid particles can move freely through a fixed computational mesh using an Eulerian approach. Fictitious boundary method (FBM) is used for treating the interaction between particles and the fluid. Hydrodynamic forces acting on the particle's surface are calculated using an explicit volume integral approach. A collision model proposed by Glowinski, Singh, Joseph and coauthors is used to handle particle-wall and particle-particle interactions. The particulate flow is computed using multigrid finite element solver FEATFLOW. Numerical experiments are performed considering two particles falling and colliding and sedimentation of many particles while interacting with each other. Results for these experiments are presented and compared with the reference values. Effects of the particle-particle interaction on the motion of the particles and on the physical behavior of the fluid-particle system has been analyzed.
https://doi.org/10.1063/1.5035163

I. INTRODUCTION

Particulate flows have broad applications in industry such as fluidized suspensions, hydraulic fracturing of reservoirs, lubricated transport, paper pulp, slurry flow, food products etc. These types of flows are common in many naturally occurring processes such as wind blown sand flow or dust particles in air, interaction between ocean current and offshore structures, lava flow and sedimentation in estuary etc. Motion of solid particles in fluids are somewhat complex and difficult to simulate especially from a numerical point of view because frequent deformation and generation of computational grid is required in many cases when the particle have complex boundaries which are moving with time. The problem gets more complex due to particle-particle and particle-wall collisions in case of a large number of particles as well as fluid particle interactions get complicated.

A lot of numerical simulation techniques have been developed to simulate such flows such as level-set methods,[17,19] penalty based method,[23] discrete element models (DEM),[15,16,20] population balance based models[2,4] and distributed Lagrange multiplier (DLM) fictitious domain methods.[6,12,18,24] In these methods, continuity and momentum equations govern the fluid flow and the motion of particles are modeled by the Newton-Euler equations. The flow field around each particle is resolved to obtain the hydrodynamic forces and torques acting on the particles. These methods can be broadly classified into two groups. The first one is based on an Eulerian approach which uses a fixed mesh. The mesh covers the whole domain occupied by the fluid and is independent of the solid particles. A famous example of this approach is the fictitious domain method proposed by Glowinski,

[a]E-mail: kamran.usman@mail.au.edu.pk, khuram.walayat@pku.edu.cn, rashid.mahmood@mail.au.edu.pk and nabeela@mail.au.edu.pk

Joseph and coauthors.[6,18,24] The second one is a Lagrangian approach, in which the moving mesh follows the moving particle boundaries in the fluid. Due to the arbitrary motion of the mesh within the fluid, this approach is usually refferred to as Arbitrary Lagrangian Eulerian (ALE).[7,9,13,22,30] Maury,[13] Hu, Joseph and coauthors[8] have frequently used the ALE for particulate flows. A great advantage of Eulerian approach over the Lagrangian approach is that there is no need to change the computational mesh which significantly decreases per time step cost of CPU. Hence, less computational effort is required by saving the costly mesh generation process but that may affect the resulting accuracy. Therefore, the overall aim in all of these methods is to successfully deal with the moving boundaries in the fluid while the accuracy of the numerical approximation is acceptable and at the same time the computational cost is less.

Collisions or nearly a collision between particles in fluid can produce serious difficulties in the direct simulation of solid liquid flows. When the particles are close to each other, the flow fields in the narrow gap between the converging particle surfaces have to be resolved accurately which increases the cost of simulation significantly. In Lagrangian approaches the corresponding element size has to be reduced, resulting in more number of unknowns to be solved for. Moreover, numerical problems are likely to occur when particles are close to each other and the gap zone between the particles has to be refined which makes the method computationally expensive. Such problems are treated using a collision model which prevents particles from inter-penetrating or getting to close to each other. In literature, different collision models have been proposed to handle particle collisions numerically such as lubrication models,[14] repulsive models,[32] conservation of linear momentum and kinetic energy,[35] stochastic collision models[25] and semi-experiential collision models, etc. Singh, Hesla and Joseph[24] used a repulsive model in which collision force is initiated only when the particle boundaries overlap or touch which allows the particles to experience the hydrodynamic lubrication forces up to the full tolerance of the mesh and the particles can pack naturally in equilibrium. We use a repulsive force model proposed by Glowinski, Joseph and coauthors[18] which prevents particle collisions and can also deal with the case of overlapped particles due to unavoidable numerical truncation errors.

In this paper fictitious boundary method with an Eulerian approach has been used for the simulation of particulate flows. A volume based approach has been used to calculate the hydrodynamic drag and lift forces.[29,33] Interaction between two falling particles has been analyzed while undergoing the phenomena of drafting, kissing, tumbling and collision with each other. Sedimentation of a cluster of particles has been simulated and behavior of the settling particles has been observed.

II. MATHEMATICAL MODELLING

Consider fluid flow with N number of solid particles having mass $M_i (i = 1, 2, \cdots, N)$ and density ρ. The fluid density is ρ_f and fluid viscosity is ν. The domain occupied by fluid is $\Omega_f(t)$ and the domain occupied by the i^{th} particle is $\Omega_i(t)$. We denote the total domain as Ω_T which is given by

$$\Omega_T = \Omega_f(t) \cup \Omega_i(t) \qquad \forall i \in (1, 2, \cdots \cdot N)$$

The whole computational domain Ω_T is independent of t but Ω_f and Ω_i are always dependent on time t. We drop t in the notations and denote $\Omega_f(t) = \Omega_f$ and $\Omega_i(t) = \Omega_i$ where $\partial\Omega_i$ represents the boundary of the i^{th} particle as shown in figure 1.

A. Incompressible fluid flow model

Navier-Stokes equations govern the motion of incompressible fluid in the domain Ω_f with density ρ_f and dynamic viscosity ν[10,27,34] given by

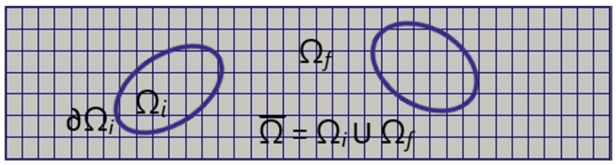

FIG. 1. Rigid particle and fluid.

$$\rho_f\left[\frac{\partial u}{\partial t}+u\cdot\nabla u\right]-\nabla\cdot\sigma=0,\quad \nabla\cdot u=0\qquad \forall\, t\in(0,T),\tag{1}$$

where σ is the total stress tensor in the fluid phase, defined as,

$$\sigma=-pI+\mu_f\left[\nabla u+(\nabla u)^T\right].\tag{2}$$

Here, fluid velocity is u, pressure is p, coefficient of viscosity is μ_f and I is the identity tensor.

B. Model of particle motion

The freely moving rigid particles in the fluid have both translational and rotational motion occurring due to hydrodynamic forces, gravitational acceleration and the particle-particle and particle-wall collision forces. Newton-Euler equations govern the motion of solid particles. If U_i and ω_i respectively are the translational and angular velocities of the i^{th} particle, then they satisfy

$$M_i\frac{dU_i}{dt}=(\triangle M_i)g+F_i+F_i',\qquad I_i\frac{d\omega_i}{dt}+\omega_i\times(I_i\omega_i)=T_i.\tag{3}$$

M_i denote the mass of the i^{th} particle and we write

$$\triangle M_i=M_i-M_f,$$

where, the mass of fluid M_f occupies the same volume as M_i. Drag and lift forces are represented by F_i which are acting on the i^{th} particle, F_i' are the particle collision forces, the moment of inertia tensor and the resultant torque acting about the center of mass of the i^{th} particle is I_i and T_i respectively, and g denotes the gravitational acceleration.

C. Fluid-particle interaction

The position X_i of the center of mass of the i^{th} particle and its angle θ_i can be obtained after integrating the following kinematic equations,[31,33]

$$\frac{dX_i}{dt}=U_i,\qquad \frac{d\theta_i}{dt}=\omega_i.\tag{4}$$

At the interface $\partial\Omega_i$, between the fluid and the i^{th} particle, we apply no-slip boundary conditions and the velocity $U(X)\forall\, X\in\bar{\Omega}_i$ is given by,

$$U(X)=U_i+\omega_i\times(X-X_i).\tag{5}$$

D. Hydrodynamic drag/lift forces and torque

The hydrodynamic drag and lift forces F_i and the torque T_i acting on the i^{th} particle's center of mass can be obtained by,[21]

$$F_i=(-1)\int_{\partial\Omega_i}(\sigma.n)d\Gamma_i,\qquad T_i=(-1)\int_{\partial\Omega_i}(X-X_i)\times(\sigma\cdot n)d\Gamma_i.\tag{6}$$

Where n is the unit normal vector drawn outwards to the boundary $\partial\Omega_i$ of the i^{th} particle.

E. Collision model

We will use a collision model for the treatment of particle-particle collisions presented by Glowinski, Joseph, Singh and coauthors[18] which is given by,

$$F_{i,j}^P=\begin{cases}0, & for\quad D_{i,j}>R_i+R_j+\rho,\\ \frac{1}{\epsilon_p}\left(X_i-X_j\right)\left(R_i+R_j+\rho-D_{i,j}\right)^2, & for\quad R_i+R_j\le D_{i,j}\le R_i+R_j+\rho,\\ \frac{1}{\epsilon_p'}\left(X_i-X_j\right)\left(R_i+R_j-D_{i,j}\right), & for\quad D_{i,j}\le R_i+R_j\end{cases}\tag{7}$$

the coordinates of the centers of the i^{th} and j^{th} particle are X_i and X_j and R_i and R_j denotes their radius respectively. The distance between X_i and X_j is $D_{i,j}=|X_i-X_j|$. ρ is the minimum distance to

activate the force of repulsion between particles. Values for the positive stiffness parameters ϵ_p and ϵ'_p are chosen as such to avoid discontinuity or singularity.

III. FICTITIOUS BOUNDARY METHOD

The fictitious boundary method (FBM)[28,31] depends on a multigrid[10,33] finite element method (FEM) based background grid comprising of the total computational domain Ω_T containing the fluid domain Ω_f and the particle domain Ω_i. The particle domain is incorporated within the fluid domain by applying the boundary conditions at the interface between the fluid and particles given by equation (5) as additional constraints to the Navier-Stokes equations. Hence, using the FBM, we can extended the fluid domain with the combined fluid and particle domain and the Navier-Stokes equations takes the form,

$$\begin{cases} \nabla \cdot u = 0 & \forall X \in \Omega_T, \\ \rho_f \left(\frac{\partial u}{\partial t} + u.\nabla u \right) - \nabla \cdot \sigma & \forall X \in \Omega_f, \\ u(X) = U_i + \omega_i \times (X - X_i) & \forall X \in \bar{\Omega}_i, (i = 1, 2, 3, \cdots, N). \end{cases} \tag{8}$$

IV. NUMERICAL COMPARISONS

In this section, we will present results of the numerical experiments performed using CFD code FEATFLOW.[26] We will analyze and observe the kinetics of particles, inside a channel, falling due to gravity. The interaction between two particles will be analyzed and the sedimentation of cluster of particles falling under the action of gravity in a fluid will be presented. First, the numerical results of two particles case with different initial positions and sizes of the particles are discussed and at the end, the results of the sedimentation of cluster of particles are presented.

In context of the particulate flow simulation of many particles, the study of particle-particle interaction effects play a very important role besides the fluid-solid interaction effects in capturing the physical behavior of the system. The particle-particle collision forces and particle interaction with each other strongly contributes to define the motion of solid particle in the fluid-particle system. In this study, we have analyzed the behavior of interacting particles keeping different configurations for the position and their sizes which affects the direction of their motion after the collisions or during the drafting, kissing and tumbling effect. A suitable distance between particles has to be maintained so that one particle can experience the wake of the other particle to trigger the process of drafting, kissing and tumbling which may lead towards the particle collisions.

For the two particle interaction case, we have kept the y-coordinate distance between the particles fixed and varied slightly the x-coordinates of the two particles for different cases in such a way that the upper particle always comes in the wake of the lower particle.

A. Two falling particles inside a channel

When we have two or more particles inside a channel flow, we need a collision model such as given by equation (2). The purpose of introducing collision model is to prevent the solid particles from interpenetrating each other. The width and height of the computational domain is 2 and 8 respectively and this domain is a channel. The particles are 2D rigid circular solid balls having density $\rho_s = 1.5$. In the numerical experiments, we consider particles of three different radii $R = 0.115$, $R = 0.125$ and $R = 0.135$. The particles are falling down in an incompressible fluid due to gravity with gravitational acceleration $g = 981$. The density of the fluid $\rho_f = 1$, it's viscosity $\nu = 10^{-2}$ and Reynolds number $Re = 100$. We consider that initially at $t = 0$ the fluid and the particles both are at rest. The simulations are performed on fixed equidistant meshes using CFD code FEATFLOW. The simulations are carried out on three different levels of mesh refinement, i.e. Level-3, Level-4 and Level-5, where number of elements on coarse mesh are 259. We use three different radii of particles with five different initial positions of the particles. The y-coordinates of the center of masses of both the particles are fixed in all the tests and we only change their x-coordinates. The y-coordinate of the center of mass of 1^{st} particle is 7.2 and of the 2^{nd} particle is 6.8. In all the tests for two circular particles falling freely inside a fluid channel, the initial positions of these particles ensures that the particles will collide during their fall and the well known phenomena of drafting, kissing and tumbling will happen.[5,8,11]

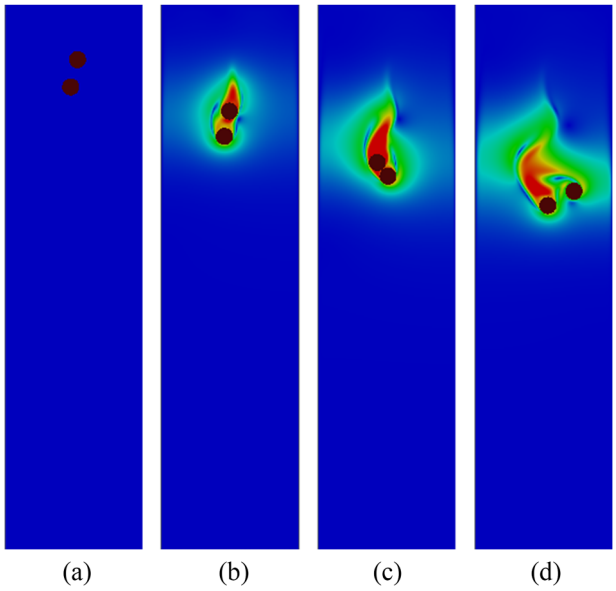

FIG. 2. Snapshots at time (a) t = 0, (b) t = 0.2, (c) t = 0.25 and (d) t = 0.3.

When two particles, placed close to each other, are dropped to fall down, the particles undergo through the process of drafting, kissing and tumbling. Figure 2 and figure 3 shows the drafting, kissing and tumbling behavior of the two falling particles along with their velocity distribution and

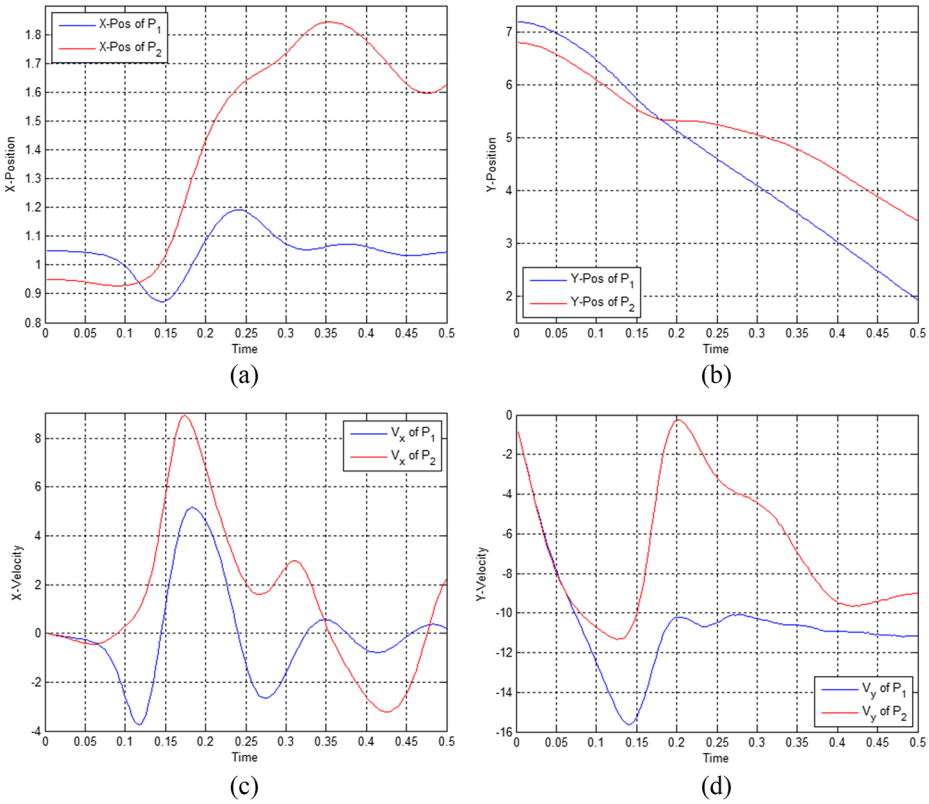

FIG. 3. Position and velocity graphs w.r.t. time. Initially upper particle is on the right side of the lower particle. (a) $x-$ *coordinate* w.r.t. time (b) $y-$ *coordinate* w.r.t. time (c) $x-$ *velocity* w.r.t. time (d) $y-$ *velocity* w.r.t. time.

TABLE I. Results for mesh level-3 with different radii and initial positions of particles.

number of elements			4144			
					after collision	
Radius	1^{st} *particle x position*	2^{nd} *particle x position*	*min distance b/w particles*	*at time*	1^{st} *particle shift*	2^{nd} *particle shift*
	1.05000	0.95000	0.0061	0.1710	Left	Right
	1.00001	0.99999	0.0018	0.1830	Left	Right
0.115	1.0	1.0	0.0	0.1560	Straight	Left
	0.99999	1.00001	0.0018	0.1830	Right	Left
	0.95000	1.05000	0.0061	0.1710	Right	Left
	1.05000	0.95000	0.0017	0.1470	Right	Left
	1.00001	0.99999	0.0	0.1500	Right	Left
0.125	1.0	1.0	0.0	0.1500	Straight	Straight
	0.99999	1.00001	0.0	0.1500	Left	Right
	0.95000	1.05000	0.0017	0.1470	Left	Right
	1.05000	0.95000	0.0036	0.1440	Right	Left
	1.00001	0.99999	0.0	0.2610	Left	Right
0.135	1.0	1.0	0.0	0.4920	Straight	Straight
	0.99999	1.00001	0.0	0.2610	Right	Left
	0.95000	1.05000	0.0036	0.1440	Left	Right

position. From figure 2, we can see that the 1^{st} particle falls with higher velocity then the 2^{nd} particle, because the 1^{st} particle is in the wake where the 2^{nd} particle is in front, therefore the hydrodynamic forces acting on the 1^{st} particle are smaller. As the particles start falling, the distance between them decreases and the particles touch (kiss) each other. After kissing, the particles start falling together until they tumble and then separate from each other. The 1^{st} particle touch the bottom first where as the 2^{nd} particle reaches the bottom later on.

We get almost similar plots for position and velocity of particles at different levels of mesh refinement with same initial positions. Therefore, here we only presents plots for Level-5 using different radii and five different initial positions of the particles. However we present the results

TABLE II. Results for mesh level-4 with different radii and initial positions of particles.

number of elements			16576			
					after collision	
Radius	1^{st} *particle x position*	2^{nd} *particle x position*	*min distance b/w particles*	*at time*	1^{st} *particle shift*	2^{nd} *particle shift*
	1.05000	0.95000	0.0017	0.1710	Left	Right
	1.00001	0.99999	0.0	0.2490	Left	Right
0.115	1.0	1.0	0.0	0.3990	Left	Right
	0.99999	1.00001	0.0	0.2490	Right	Left
	0.95000	1.05000	0.0014	0.1650	Right	Left
	1.05000	0.95000	0.0	0.2070	Left	Right
	1.00001	0.99999	0.0	0.1260	Right	Left
0.125	1.0	1.0	0.0	0.1950	Left	Right
	0.99999	1.00001	0.0	0.1260	Left	Right
	0.95000	1.05000	0.0	0.2070	Right	Left
	1.05000	0.95000	0.0	0.1860	Right	Left
	1.00001	0.99999	0.0	0.2220	Left	Right
0.135	1.0	1.0	0.0	0.1590	Straight	Right
	0.99999	1.00001	0.0	0.2220	Right	Left
	0.95000	1.05000	0.0	0.1860	Left	Right

TABLE III. Results for mesh level-5 with different radii and initial positions of particles.

number of elements			66304			
					after collision	
Radius	1^{st} *particle* *x* *position*	2^{nd} *particle* *x* *position*	*min distance* *b/w particles*	*at time*	1^{st} *particle* *shift*	2^{nd} *particle* *shift*
0.115	1.05000	0.95000	0.0189	0.1590	Left	Right
	1.00001	0.99999	0.0	0.1350	Right	Left
	1.0	1.0	0.0	0.2070	Right	Left
	0.99999	1.00001	0.0	0.1350	Left	Right
	0.95000	1.05000	0.0190	0.1590	Right	Left
0.125	1.05000	0.95000	0.0042	0.1500	Left	Right
	1.00001	0.99999	0.0	0.1860	Right	Left
	1.0	1.0	0.0	0.1920	Right	Left
	0.99999	1.00001	0.0	0.2130	Left	Right
	0.95000	1.05000	0.0042	0.1500	Right	Left
0.135	1.05000	0.95000	0.0014	0.1410	Left	Right
	1.00001	0.99999	0.0	0.4470	Straight	Straight
	1.0	1.0	0.0	0.2010	Left	Right
	0.99999	1.00001	0.0	0.2610	Left	Right
	0.95000	1.05000	0.0014	0.1410	Right	Left

for three different mesh refinement levels with three different radii and five different initial positions in Table I, Table II and Table III respectively. Although the simulations are carried out from $t = 0$ to $t = 2$, but in graphs and results we will focus the time interval from $t = 0$ to $t = 0.3$,

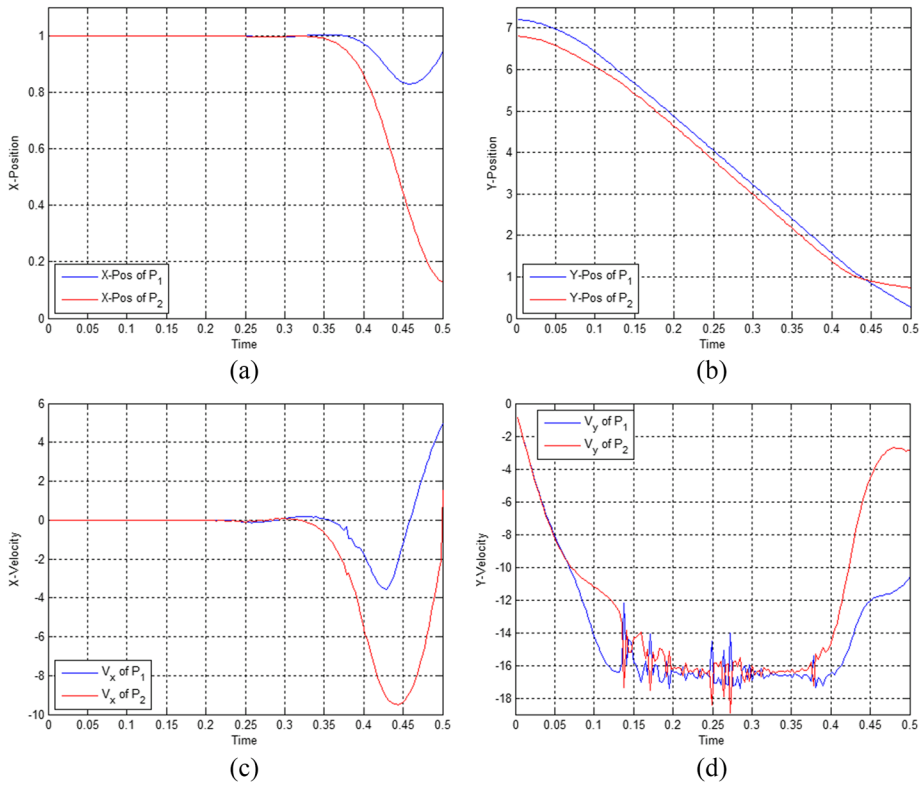

FIG. 4. Position and velocity graphs w.r.t. time. Initially upper particle is slightly on the right side of the lower particle (a) $x-$ *coordinate* w.r.t. time (b) $y-$ *coordinate* w.r.t. time (c) $x-$ *velocity* w.r.t. time (d) $y-$ *velocity* w.r.t. time.

because the process of drafting, kissing and tumbling and particle collision occurs during this time interval.

The blue line represents the first particle and the red line represents the second particle in the plots. Figure 3(a) and 3(b) shows $x-$coordinate and $y-$coordinate of the mass center of the two particles respectively, while figure 3(c) and 3(d) shows the $x-$component and $y-$component of the velocity of two particles respectively. The initial position of the mass center of the 1^{st} particle is (1.05000 , 7.2), while the initial position of the mass center of the 2^{nd} particle is (0.95000 , 6.8). We have calculated that at time $t = 0.1590$ the distance between particles become minimum and is equal to 0.0189. The 1^{st} particle shift towards the left and 2^{nd} particle towards the right after collision.

The initial position of the mass center of the 1^{st} particle is (1.00001 , 7.2), while the initial position of the mass center of the 2^{nd} particle is (0.99999 , 6.8), see figure 4. We have calculated that at time $t = 0.1350$ the distance between falling particles become minimum and is equal to zero. The 1^{st} particle shift towards the right and 2^{nd} particle towards the left after collision.

The initial position of the mass center of the 1^{st} particle is (1.0 , 7.2), while the initial position of the mass center of the 2^{nd} particle is (1.0 , 6.8), see figure 5. We have calculated that at time $t = 0.2070$ the distance between falling particles become minimum and is equal to zero. The 1^{st} particle shift towards the right and 2^{nd} particle towards the left after collision.

The initial position of the mass center of the 1^{st} particle is (0.99999 , 7.2), while the initial position of the mass center of the 2^{nd} particle is (1.00001 , 6.8), see figure 6. We have calculated that at time $t = 0.1350$ the distance between falling particles become minimum and is equal to zero. The 1^{st} particle shift towards the left and 2^{nd} particle towards the right after collision.

The initial position of the mass center of the 1^{st} particle is (0.95000 , 7.2), while the initial position of the mass center of the 2^{nd} particle is (1.05000 , 6.8), see figure 7. We have calculated that at time $t = 0.1590$ the distance between falling particles become minimum and is equal to 0.0190. The 1^{st} particle shift towards the right and 2^{nd} particle towards the left after collision.

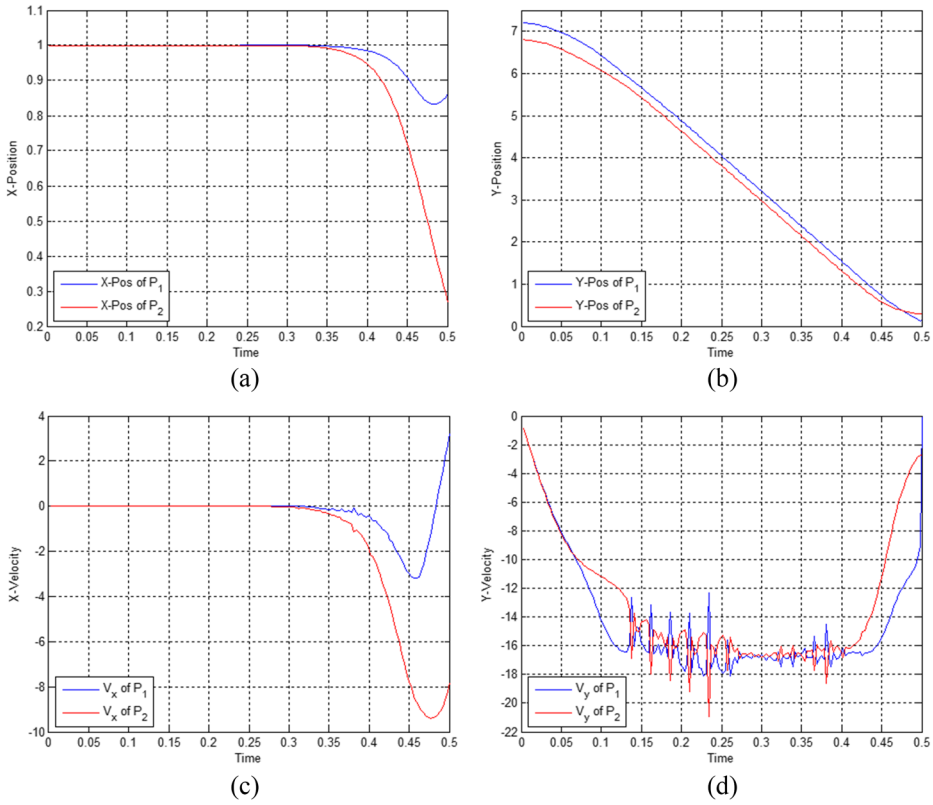

FIG. 5. Position and velocity graphs w.r.t. time. Initially upper and lower particle have the same x-position (a) $x-$ *coordinate* w.r.t. time (b) $y-$ *coordinate* w.r.t. time (c) $x-$ *velocity* w.r.t. time (d) $y-$ *velocity* w.r.t. time.

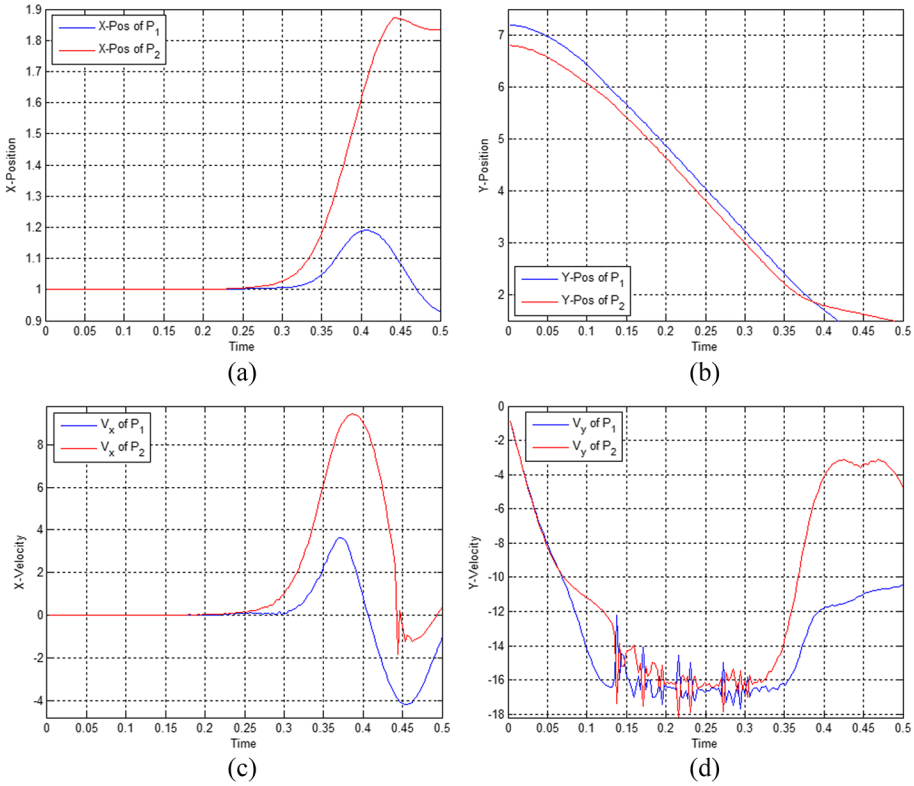

FIG. 6. Position and velocity graphs w.r.t. time. Initially upper particle is slightly on the left side of the lower particle (a) $x-$ *coordinate* w.r.t. time (b) $y-$ *coordinate* w.r.t. time (c) $x-$ *velocity* w.r.t. time (d) $y-$ *velocity* w.r.t. time.

Now we presents the data in tables to show the results of two falling particles inside a channel, for different levels of mesh refinement, with different radii and initial positions of the particles. We analyze and observe the process of drafting, kissing and tumbling along with the collision of particles, using mesh Level-3, Level-4 and Level-5, where the number of elements on coarse mesh are 259. The Table I, Table II and Table III clearly shows the obtained results for three different radii of particles and five different initial positions of the particles. The $y-$coordinate of the initial positions of the two particles are fixed and we only vary $x-$coordinates of their initial positions. Table I presents the results for numerical experiments performed using mesh refinement of Level-3.

The Table I clearly shows that when we change the initial positions of the particles, the behavior of the particles during their fall is different. Moreover, the particles show different behavior when we change their size. For example, if we consider the same initial positions, i.e., $x = 1.05000$ of 1^{st} particle and $x = 0.95000$ of 2^{nd} particle. The minimum distance between particles is 0.0061 at time $t = 0.1710$, when the radius of the particles is $R = 0.115$ and the 1^{st} particle shifts towards left after collision while the 2^{nd} particle moves towards right. But when the radius of the particles is $R = 0.125$, with same initial positions the minimum distance between particles becomes 0.0017 at time $t = 0.1470$ and the 1^{st} particle drifts toward right whereas the 2^{nd} particle shifts towards left, after the collision process. Similarly when the radius is $R = 0.135$ with same initial positions of the particles the minimum distance between them is 0.0036 at time $t = 0.1440$.

All the numerical experiments carried out for mesh Level-3 are performed on mesh refinement Level-4. Table II presents the results obtained by simulating these numerical experiments on mesh Level-4. Whereas, the number of elements on Level-4 are 16576.

Table II shows that the minimum distance between particles decreases and is zero for almost all the cases, when simulations are carried out on mesh Level-4. A similar behavior of particles as on Level-3 can be observed on Level-4, i.e., the trajectories of these particles depend on their initial positions and also on the size of particles. When we change the initial positions of the particles, the particles follow different paths during their fall. The particles also change their path when the size of

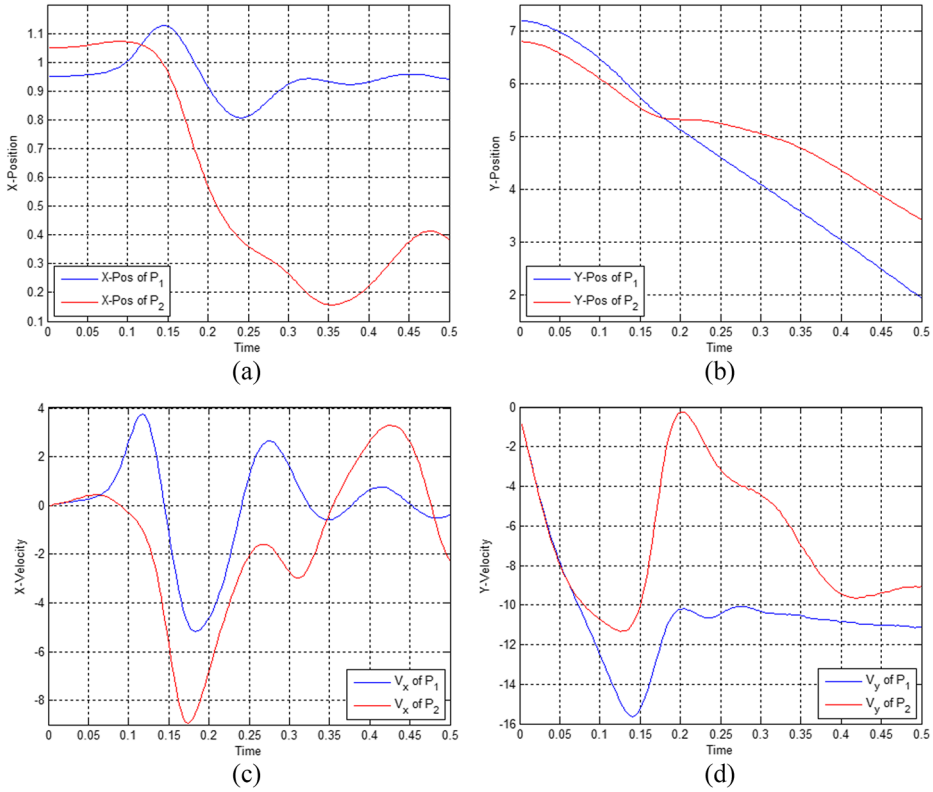

FIG. 7. Position and velocity graphs w.r.t. time. Initially upper particle is on the left side of the lower particle (a) $x-$ *coordinate* w.r.t. time (b) $y-$ *coordinate* w.r.t. time (c) $x-$ *velocity* w.r.t. time (d) $y-$ *velocity* w.r.t. time.

the particles is changed with same initial positions of the particles. Thus, it shows that the paths of the particles during their downward fall also depends on the initial distance between the particles.

Again we can see that the behavior of the particles depend on the initial positions and size of the particles as well as on the mesh refinement level (Table III).

B. Sedimentation of cluster of particles

Finally, we consider the sedimentation of many particles initially in the form of cluster. We take 80 circular particles falling down inside a rectangular channel, each particle is of same size. The width of the channel is 4 and it's height is 6. The radius of each particle is $R = 0.1$. These 80 particles are placed such that they form a cluster at the top of the channel at time $t = 0$, as shown in figure 8. The density of each particles is $\rho_s = 1.5$. The density of the fluid is $\rho_f = 1$ and the viscosity

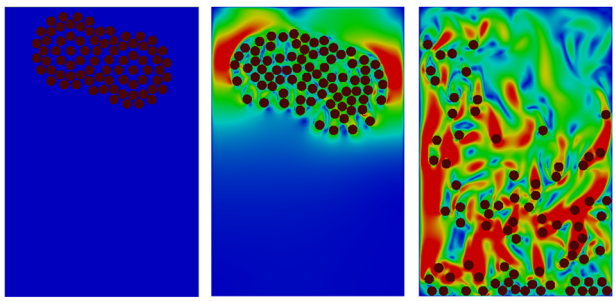

FIG. 8. Snapshots at time t = 0, t = 0.1, t = 0.6 (from left to right).

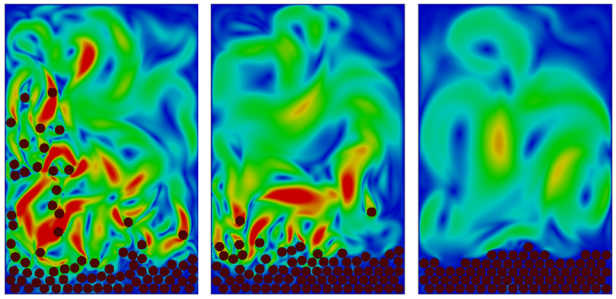

FIG. 9. Snapshots at time t = 0.9, t = 1.2, t = 1.7 (from left to right).

of the fluid is $\nu = 10^{-2}$, where the Reynolds number is $Re = 100$. Consider that both fluid and particles are at rest at $t = 0$. We chose the range of repulsive force $\rho = 0.0365$. Where as, we use the value of parameter $\epsilon_p = 10^{-6}$ in the collision model given by equation (2).

The sedimentation of the cluster of the particles is shown in Figure 8 and figure 9. These figures clearly shows the development of Rayleigh-Taylor instability. This instability develops into a viscous fingering phenomenon, and exhibits many other phenomenon such as symmetry breaking, bifurcation phenomena and the drafting, kissing and tumbling effect which takes place at various scales in space and time. We can observe the formation of many complex vortices of different sizes which causes the particles to pull in different directions and mix them with each other making the whole process very chaotic. At the end, all the particles settle down at the bottom of channel and the fluid again comes to rest.

V. CONCLUSION

In this work we have employed a direct simulation technique to simulate the particulate flows using the multigrid fictitious boundary method (FBM). The main focus of the presented work is to study the behavior and interaction of particles with each other and with the fluid. We have observed and examined two circular particles falling and colliding inside a channel with the effect of gravity and the hydrodynamic forces acting on the particles and sedimentation of a cluster of particles.

The main advantage of the used FBM is that the computational mesh has not to change with time which saves the expensive mesh generation and hence less computational effort is required. The mesh is chosen independent of the solid particles i.e., the solid particles having different shape, size and number are allowed to move freely through the computational mesh. The hydrodynamic forces acting on the moving particles are calculated using a volume based approach.

A collision model based on the papers presented by Glowinski, Joseph, Singh and coauthors is used to handle the particle-particle and particle-wall interactions. This model applies short range repulsive forces between the neighboring/colliding particles which prevent the particles to come very close to each other and collide. Another advantage of this collision model is that it can handle the situation when the particles overlap due to numerical errors. For handling sedimentation of a large number of particles, the used collision model is very effective.

The presented results for two circular particles falling under the action of gravity inside a channel showed different behaviors for different starting positions of the particles. Moreover, we concluded that size of the particle plays a significant role in defining particle's path during drafting, kissing and tumbling. The results were compared with different mesh refinement levels. The analysis was performed by taking five different initial positions for the upper particle and three different radii were chosen at three different mesh refinement levels. The minimum distance between the particles and the time when the distance between the particles become minimum during the collision process and their path during they separate was observed and conclusions were made. At the end, the sedimentation of a cluster of 80 particles is simulated and its results are presented. During the sedimentation, many complex vortices of different sizes were formed, these vortices pull the particles in different directions

and mix them with each other and at the end, all the particles settle down at the bottom and the fluid comes to rest again.

In future, we plan to compare and analyze the presented numerical experiments using different Reynold's number and for particles of arbitrary shape other than circular one that we used in the presented numerical tests. Some improved collision models can be tested in case of many packed particles during sedimentation, when the number of particles reaches over 1000 and it becomes difficult to handle particle collisions. We also intend to extend the results to 3D which is a very promising task. It will be worthwhile to consider electrical interactions, Van der Waals forces and coagulation of particles[1,3] by using the Arbitrary Lagrangian Eulerian approach.

[1] N. Afshar-Mohajer, C.-Y. Wu, and N. Sorloaica-Hickman, "Efficiency determination of an electrostatic lunar dust collector by discrete element method," Journal of Applied Physics **112**(2), 023305 (2012).

[2] E. Bayraktar, O. Mierka, F. Platte, D. Kuzmin, and S. Turek, "Numerical aspects and implementation of population balance equations coupled with turbulent fluid dynamics," Computers & Chemical Engineering **35**(11), 2204–2217 (2011).

[3] J. Cordelair and P. Greil, "Discrete element modeling of solid formation during electrophoretic deposition," Journal of Materials Science **39**(3), 1017–1021 (2004).

[4] T. J. Crowley, E. S. Meadows, E. Kostoulas, and F. J. Doyle III, "Control of particle size distribution described by a population balance model of semibatch emulsion polymerization," Journal of Process Control **10**(5), 419–432 (2000).

[5] A. F. Fortes, D. D. Joseph, and T. S. Lundgren," Nonlinear mechanics of fluidization of beds of spherical particles," Journal of Fluid Mechanics **177** (1987).

[6] R. Glowinski, T. W. Pan, T. I. Hesla, and D. D. Joseph, "A distributed Lagrange multiplier/fictitious domain method for particulate flows," International Journal of Multiphase Flow **25**(5), 755–794 (1999).

[7] C. W. Hirt, A. A. Amsden, and J. L. Cook, "An arbitrary Lagrangian-Eulerian computing method for all flow speeds," Journal of Computational Physics **14**(3), 227–253 (1974).

[8] H. H. Hu, D. D. Joseph, and M. J. Crochet, "Direct simulation of fluid particle motions," Theoretical and Computational Fluid Dynamics **3**, 285–306 (1992).

[9] H. H. Hu, N. A. Patankar, and M. Y. Zhu, "Direct numerical simulations of fluid-solid systems using the arbitrary Lagrangian-Eulerian technique," Journal of Computational Physics **169**(2), 427–462 (2001).

[10] V. John, "Higher order finite element methods and multigrid solvers in a benchmark problem for the 3D Navier-Stokes equations," Int. J. for Numerical Methods in Fluids **40**, 775–798 (2002).

[11] A. A. Johnson and T. E. Tezduyar, "Simulation of multiple spheres falling in a liquid-filled tube," Computer Methods in Applied Mechanics and Engineering **134**, 351–373 (1995).

[12] K. Usman, K. Walayat, Z. Wang, and M. Liu, "A multigrid finite element fictitious boundary method for fluid-solid two-phase flows," The 8th International Conference on Computational Methods (ICCM2017) (Advances in Computational Engineering Science, ed.), ScienTech Publisher, 2017.

[13] B. Maury, "Characteristics ALE method for the unsteady 3D Navier-Stokes equations with a free surface," International Journal of Computational Fluid Dynamics **6**, 175–188 (1996).

[14] B. Maury, "A many-body lubrication model," J. for Comput. and Appl. Math. **325**(9), 1053–1058 (1997).

[15] B. K. Mishra and R. K. Rajamani, "The discrete element method for the simulation of ball mills," Applied Mathematical Modelling **16**(11), 598–604 (1992).

[16] A. Munjiza, D. R. J. Owen, and N. Bicanic, "A combined finite-discrete element method in transient dynamics of fracturing solids," Engineering Computations **12**, 145–174 (1995).

[17] S. Osher and R. P. Fedkiw, "Level set methods: An overview and some recent results," Journal of Computational Physics **169**(2), 463–502 (2001).

[18] N. A. Patankar, P. Singh, D. D. Joseph, R. Glowinski, and T. W. Pan, "A new formulation of the distributed Lagrange multiplier/fictitious domain method for particulate flows," Int. J. Multiphase Flow **26**, 1509–1524 (2000).

[19] S. B. Pillapakkam and P. Singh, "A level-set method for computing solutions to viscoelastic two-phase flow," Journal of Computational Physics **174**(2), 552–578 (2001).

[20] A. V. Potapov, M. L. Hunt, and C. S. Campbell, "Liquid-solid flows using smoothed particle hydrodynamics and the discrete element method," Powder Technology **116**(2-3), 204–213 (2001).

[21] S. Kim and S. J. Karrila, *Microhydrodynamics: Principles and selected applications*, second ed. (Butterworth-Heinemann, Boston, 1991).

[22] J. Sarrate, A. Huerta, and J. Donea, "Arbitrary Lagrangian-Eulerian formulation for fluid-rigid body interaction," Computer Methods in Applied Mechanics and Engineering **190**(24), 3171–3188 (2001), Advances in Computational Methods for Fluid-Structure Interaction.

[23] A. Sarthou, S. Vincent, J. P. Caltagirone, and Ph. Angot, "Eulerian-Lagrangian grid coupling and penalty methods for the simulation of multiphase flows interacting with complex objects," International Journal for Numerical Methods in Fluids **56**(8), 1093–1099 (2008).

[24] P. Singh, T. I. Hesla, and D. D. Joseph, "Distributed Lagrange multiplier method for particulate flows with collisions," International Journal of Multiphase Flow **29**(3), 495–509 (2003).

[25] M. Sommerfeld, "Validation of a stochastic Lagrangian modelling approach for inter-particle collisions in homogeneous isotropic turbulence," International Journal of Multiphase Flow **27**(10), 1829–1858 (2001).

[26] S. Turek, Featflow. finite element software for the incompressible navier-stokes equations: User manual, release 1.1., Tech. report, 1998.

[27] S. Turek, "Numerical analysis of a new time-stepping θ-scheme for incompressible flow simulations," *Ergebnisberichte angewandte Mathematik*, Univ. Dortmund, Fachbereich Mathematik, 2005.

[28] S. Turek, D. Wan, and L. S. Rivkind, "The fictitious boundary method for the implicit treatment of Dirichlet boundary conditions with applications to incompressible flow simulations," *Challenges in Scientific Computing - CISC 2002* (E. Baensch, ed.), Lecture Notes in Computational Science and Engineering, vol. 35, Springer Berlin Heidelberg, 2003, pp. 37–68 (English).
[29] K. Usman, "Numerical analysis of collision models in 2d particulate flow," Ph.D. thesis, Technische Universität Dortmund, Fakultät für Mathematik, 2013.
[30] D. Wan and S. Turek, "Fictitious boundary and moving mesh methods for the numerical simulation of rigid particulate flows," Journal of Computational Physics **222**(1), 28–56 (2007).
[31] D. Wan and S. Turek, "Direct numerical simulation of particulate flow via multigrid fem techniques and the fictitious boundary method," International Journal for Numerical Methods in Fluids **51**(5), 531–566 (2006).
[32] D. Wan and S. Turek, "An efficient multigrid-fem method for the simulation of solid-liquid two phase flows," Journal of Computational and Applied Mathematics **203**(2), 561–580 (2007).
[33] D. Wan, S. Turek, and L. S. Rivkind, "An efficient multigrid fem solution technique for incompressible flow with moving rigid bodies," *Numerical Mathematics and Advanced Applications* (M. Feistauer, V. Dolejsi, P. Knobloch, and K. Najzar, eds.), Springer Berlin Heidelberg, 2004, pp. 844–853 (English).
[34] J. F. Wendt (ed.), *Computational Fluid Dynamics*, Springer Berlin Heidelberg, 2009.
[35] N. Zhang and Z. C. Zheng, "A collision model for a large number of particles with significantly different sizes," J. Phys. D: Appl. Phys. **40**, 2603–2616 (2007).